coatings

MDPI

Review

Application of Computer Calculation in the Study of Grain Boundary

Longfei Pu, Chengxuan Peng, Min Zhu *, Yan Li * and Longxian Li

College of Nuclear Science and Technology, Naval University of Engineering, Wuhan 430033, China; 13730918574@163.com (L.P.); pcx16744@163.com (C.P.); lilongxian0623@126.com (L.L.)
* Correspondence: min0zhu@163.com (M.Z.); yacareft@163.com (Y.L.)

Abstract: A grain boundary (GB) is a structure of great concern in materials research, which affects the mechanical properties and electrical conductivity of materials, but the microscopic thermodynamic properties of GBs cannot be explained comprehensively. In this review, we demonstrate a variety of calculation methods for GBs: density functional theory (DFT) and molecular dynamics (MDs) aim to extract the thermodynamic and kinetic properties of GBs on the atomic scale, and machine learning accelerates DFT or improves the accuracy of MDs. These methods explain the microscopic properties of a GB from different perspectives and are combined by machine learning. It is hoped that this review can inspire new ideas and provide more practical applications of computer calculations in GB engineering.

Keywords: GB; computer calculation; machine learning

1. Introduction

Metal atoms are bonded by metallic bonds. According to theoretical calculations, the strength of a metal should be two to three orders of magnitude higher than what it actually exhibits. However, in materials, there are a large number of microscopic defects between metal atoms, such as vacancies, interstitials, impurities, dislocations, grain boundaries (GBs) and phase boundaries, the presence of which reduces the strength of the material. GBs are widely present in polycrystalline materials, which can be regarded as planar surfaces consisting of multiple edge-type dislocations. On the one hand, GBs hinder the movement of dislocations and provide higher strength compared to the lattice; on the other hand, GBs are more energetic and tend to be enriched with magazine atoms, resulting in faster corrosion rates than ordered structures. With the development of industry and computer calculations, the properties of GBs have consistently been a subject of interest. GB engineering and other materials science problems need to analyze them existing in polycrystalline materials, but the databases cannot satisfy the demand of exploring the details of GBs and explaining the mechanism of their influence on macroscopic properties [1].

Computer calculations are one of the important methods to explore the properties of GBs in materials, and numerical simulations are more economical under the premise of accuracy. We hope to explain and predict the properties of GBs and explore their application possibilities through calculations. In the research of the multi-scale design of novel Co-based alloys by Liu Xingjun et al. [2], it can be seen that a relatively complete thermodynamic data acquisition method has been formed for the multi-component Co-based alloys, and the data of binary alloys can be effectively supplemented by the first principle [3], which can sift materials using a high-throughput method. CALPHAD and the phase-field method can solve the problem of inconsistency between the model and the thermodynamic parameters. However, there is still a problem in the kinetic data. Some of the exchange-correlation functionals are quite different from the experimental values in the calculation of diffusion coefficients [4], which are focused on in the study of solid solutions.

check for updates

Citation: Pu, L.; Peng, C.; Zhu, M.; Li, Y.; Li, L. Application of Computer Calculation in the Study of Grain Boundary. *Coatings* **2024**, *14*, 815. https://doi.org/10.3390/coatings14070815

Academic Editor: Alexander Tolstoguzov

Received: 22 May 2024
Revised: 21 June 2024
Accepted: 22 June 2024
Published: 30 June 2024

The article found that machine learning methods can effectively accelerate the work in this field and have great potential for the improvement of material databases.

Based on some of the DFT calculations of materials that our group have performed [5,6], we found that the computational cost associated with DFT forces us to find new methods to perform more comprehensive calculations on the research objects as we go deeper into this study. In this review, we investigate the first principles, molecular dynamics and machine learning methods to find a more economical and accurate research process for the in-depth study of GB materials. Currently, the first principle algorithms are continuously optimized and machine learning methods are being updated [7]. We will focus on the application and development of the first nature principle and machine learning potential (MLP) for the prediction of GB properties.

2. Application in GB Structure

2.1. Simulation Calculations Based on First Principles

First principles calculation denotes the calculation method that directly predicts various physicochemical properties of materials from their electronic structures according to the theory of quantum mechanics. This is currently an effective method for scientific research and has been applied in many fields, such as materials, biology and condensed matter physics, as it is complementary to experimental observation [8,9]. First principles calculations take elementary species and lattice information as data and use density flood theory to realize the solution of Schrödinger's equation to obtain the macroscopic properties of materials. A computational simulation can be summarized into two main roles: one is to predict the material structure and explore the material properties [10,11]; the other is to explain the experimental phenomena and investigate the reaction mechanism [8–11].

Grain boundaries, as a type of inherent defect in materials, introduce lattice mismatches and excess volume that significantly affect material properties and behavior, including electrical conductivity, thermal conductivity, corrosion resistance, migration and solute segregation [12,13]. In order to improve materials, it is imperative to model grain boundaries and investigate the effects of grain boundary geometry and an electronic structure on material properties and behavior from an atomic scale [14–16].

In the grain boundary, there is a transition in the arrangement from one direction to another; therefore, the atomic arrangement at the grain boundary is irregular. This leads to the grain boundary exhibiting different properties compared to the grain. Metal impurities are often easily enriched in the grain boundaries [17,18]. Grain boundaries are prone to vacancy defects affecting the material's electrical conductivity [19]. Hydrogen, carbon dioxide, water and other molecules preferentially dissociate at the grain boundaries, via adsorption and diffusion, enabling the grain boundary to function as a "channel" for material corrosion [20]. In summary, the influence of the grain boundary on the material is critical, the study of the grain boundary is also necessary, and the first step is to fully comprehend the structure of the grain boundary. In a two-dimensional lattice, the grain boundary can be indicated by the angle and orientation difference of two grains, while in a three-dimensional lattice, the grain boundary is more complicated and needs to be projected in different planes and comprehensively indicated. In 1975, H. Grimmer proposed the theory of a coincident site lattice (CSL) [21], and the initial grain boundary model constructed by this has been widely used in the field of grain boundary research. The grain boundary allows for the recombination of the lattice between two grains, allowing them to undergo extended rotation relative to each other. Some of the atoms exhibit regular coincidence, and these coincident positions of the atoms form a new lattice known as the recombination lattice. The recombination dot matrix model is based on the periodicity and interactions of crystals and is used to describe the structure and properties of crystals, which in turn leads to large-scale calculations and simulations to predict the physical and chemical properties of crystals.

The specific structure of the $\sum 5(021)/[100]$ crystal boundary is given in the following Figure 1.

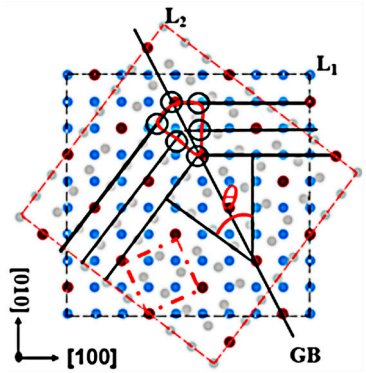

Figure 1. ∑5(021)/[100] grain boundary.

As in the above figure, the blue dot matrix L1 is rotated by an angle according to the [100] axis to obtain the gray dot matrix L2. The overlapping part is the brick red dot matrix, taking the brick red dot matrix as the grain boundary, the blue dot matrix on one side and the gray dot matrix on the other side, which is an overlapping dot matrix model. Every 5 pairs of dot matrixes in the figure have one pair of overlap, so the overlap is 1/5, the number of the overlap is ∑ = 5, the grain boundary is a ∑5 grain boundary, the axis of rotation is [001] and the grain interface is (210). In the cubic crystal system, the symmetric tilted grain boundary can be expressed as ∑ (*h k l*), where (*h k l*) is the Miller index of the grain boundary, and ∑ can be calculated from the Miller index of the grain interface [22]:

$$\sum = \delta\left(h^2 + k^2 + l^2\right) \quad (1)$$

If $h^2 + k^2 + l^2$ is odd, $\delta = 1$, and if $h^2 + k^2 + l^2$ is even, $\delta = 0.5$. The grain boundary models mentioned in this paper are all based on the theory of the coincident site lattice. Emeric Bourasseau et al. [22]. for the first time investigated the atomic structure of two symmetrically tilted grain boundaries in uranium dioxide bicrystals by combining high-resolution transmission electron microscopy (HR-TEM) and atomic-scale numerical simulations and found excellent agreement between experimental observations and simulated structures (Figure 2).

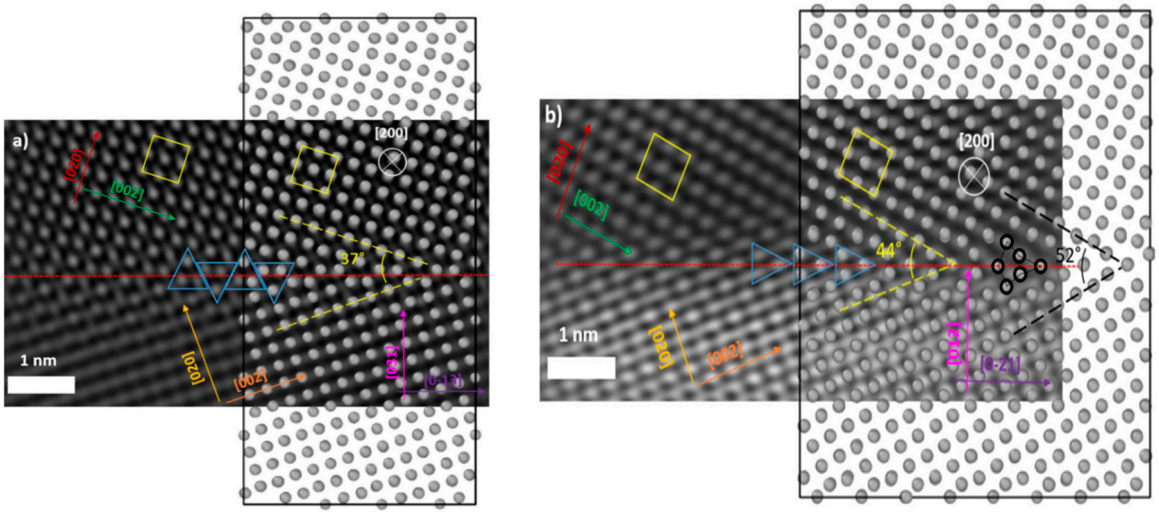

Figure 2. The comparison between the HR-TEM images and simulated systems for the ∑5(031)/[100] −36.86 (**a**) and ∑5(021)/[100] − 53.13 (**b**). Only uranium atoms are displayed on the simulation snapshots. The red dotted lines indicate the GB interfaces. The yellow and black dotted lines allow for visualizing the misorientation angles. The arrows indicate various axes. The yellow squares represent the FCC lattice, and the blue triangles reveal the atomic patterns at the GB interface. The black circles on figure (**b**) show the structural unit of a fluorite.

The recombination dot matrix model is the basic method for constructing grain boundaries, but to understand the effect of grain boundaries on material properties, the specific structure of grain boundaries needs to be investigated, from which various models have been derived, including the structural unit model [5,16,19], the coordination number [23] and other methods. Structural units are identical structures that appear periodically on grain boundaries, and they play an important role in the representation and identification of grain boundary structures. Ashby et al. [24] demonstrated, based on the rigid sphere model, that nine convex triangular polyhedra can describe the structure of all grain boundaries. Dickey et al. [25] determined by Z-contrast imaging microscopy that two symmetric yttria-stabilized cubic zirconia through Z-contrast imaging microscopy tilted [001] grain boundaries and found that both boundaries consisted of periodic arrays of elementary grain boundary structural units whose atomic structures were determined from Z-contrast images. Hajime Hojo et al. [26] used scanning transmission electron microscopy, electron energy-loss spectroscopy and first principles calculations to determine the $\sum$5(210) grain boundary Ce and oxygen sublattices of CeO_2. This finding paves the way for a comprehensive understanding of grain boundaries through the atomic-scale determination of the atomic and defect positions. The adaptation of structural units in the description of grain boundaries is determined at the level of experimental observations and theoretical calculations by mutually verifying scanning transmission electron microscopy and first principles calculations.

The coordination number, in coordination chemistry, is the number of coordinating atoms around the central atom in a compound, a concept first introduced in 1893. In crystallography, the coordination number is the number of lattices in the crystal lattice that are closest to a particular Bravais lattice, and the rest of the grain boundary structure or cell type is used to determine how closely the atoms are stacked. Jiake Wei et al. [27] combined valence electron energy-loss spectroscopy (EELS) with first principles calculations and found that a decrease in the forbidden bandwidth at the grain boundaries is directly correlated with a decrease in the number of coordinating atoms of the Al and O ions at the grain boundaries. In addition to the coordination number, M. Imaeda used dangling bonds and structural distortions to characterize the structural deformation at the grain boundaries.

Due to the loose structure of grain boundaries, they become channels for the diffusion of gas molecules. The interaction between grain boundaries and molecules can be summarized using three processes: adsorption, diffusion and polarization. At this stage, there are fewer studies on gas adsorption at grain boundaries, and most of them are studies on the adsorption of gas molecules (e.g., H_2, CO, CO_2, H_2O, etc.) on the surface of the body. H.L. Yu et al. [28] used DFT to calculate hydrogen atom adsorption and diffusion on the PuO_2 (110) surface. A conventional approach to study atom adsorption and diffusion using DFT is to identify stable adsorption sites, which adsorb from the surface to the body, and then use the Climbing Image-Nudged Elastic Band (C-NEB) to find the minimum energy path between several adsorption sites.

This involves the adsorption energy, which is calculated as follows:

$$E_{ads} = E_{M/N} - E_M - E_N \quad (2)$$

where $E_{M/N}$ is the energy of the total system with adsorbed M atoms, E_M is the energy of the M atoms and E_N is the initial total energy of the N system.

The first principle is applied to achieve more molecular adsorption at grain boundaries and less diffusion and segregation. The reasons for this are, firstly, the model construction is difficult, and the calculation is large; secondly, the density functional theory calculation is difficult to use to simulate the dynamic process of the particles. Even if the study of dynamic processes such as diffusion and polarization is aimed at the calculation of the initial and final states, the study of the transition state is lacking. Theoretical calculations based on the first principle and molecular dynamics have their own advantages and disadvantages: DFT can more accurately calculate the electronic structure and properties of the material, but it requires large computational resources and high-performance servers; molecular dynamics

is suitable for large-scale systems and long time scale processes and has advantages in the study of the dynamic behavior and mechanical properties of materials. Therefore, both DFT and molecular dynamics are indispensable tools for the study of materials, and they can complement each other.

2.2. Molecular Dynamics Calculations of Kinetic Properties

The structure and energy of equilibrium GBs constitute a thermodynamic study; however, it is difficult to reach equilibrium at the GBs in polycrystals, so dynamics issues such as the evolution of GBs in polycrystalline materials need to be investigated. A kinetic analysis of GBs is of great importance, and by gaining access to the evolution of the microstructure, it is possible to explain the way in which materials evolve during processing on larger scales and their effect on the behavior of crystal defects [29].

GB mobility is an important kinetic property in the evolution of polycrystalline microstructures, and GB mobility is defined (1) as the ratio of the GB velocity v to the thermodynamic driving force (per area) F in the limit of infinitesimal driving force [29],

$$M = \lim_{F \to 0} \frac{v}{F} \tag{3}$$

The motion of GBs changes the average size of the crystals and also affects the electrical, optical and mechanical properties. The control of GB motions has become an effective means of regulating polycrystalline properties in materials processing [30], so it is necessary to analyze the crystal evolution process and its influencing factors.

The way to control the rate of microstructure evolution is to control the change in temperature (T)—the annealing process; therefore, lots of grain boundary mobility studies have been carried out based on temperature. Kongtao Chen and Jian Han et al. used the kinetic Monte Carlo method (kMC) to perform simulations of a quasi-2D bicrystal structure [31] and statistically formed a mechanical model and validated it with MDs, which explains the variation in grain boundary mobility with temperature. The statistical disconnection (i.e., line defect) model developed in the study reveals that the temperature dependence of grain boundary mobility is related to the different dynamics of the line defects at low and high temperatures: at low temperatures, the grain boundaries consisting of a single type of fracture follow the Arrhenius formula as shown in Figure 3, and at high temperatures, the mobility is inversely proportional to the temperature, which proves the phenomenon of "anti-heat" in the macroscopic state [32].

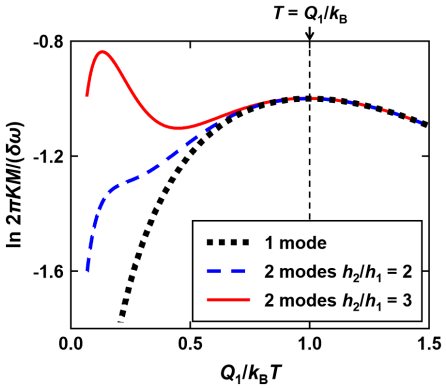

Figure 3. The temperature dependence of GB mobility for a single mode (black dotted curve), two modes with *h2/h1* = 2 < e (blue dashed curve) and two modes with *h2/h1* = 3 > e (red solid curve) cases. In the two-mode simulations, $Q_2 = 10Q_1$. The *x*-axis represents the temperature when the contribution of the long-range elastic interactions is much smaller than the estimate of the disconnection core energy (T→0), and the *x*-axis represents GB mobility in classical Arrhenius coordinates.

In this article, static relaxation calculations as well as single-point energy calculations have been performed for two specific grain boundaries in aluminum, and thermodynamic parameters are used to determine the energy distribution associated with fracture motion

when using EAM potential calculations, providing parameterizations for the kMC and statistical disconnection kinetic theory as shown in Figure 4. The kMC and fracture models are later compared with the molecular dynamics simulations of grain boundary migration, and all three results were found to be in good agreement, implying that both the kMC and the theory can be used to qualitatively predict the migration behavior of GBs.

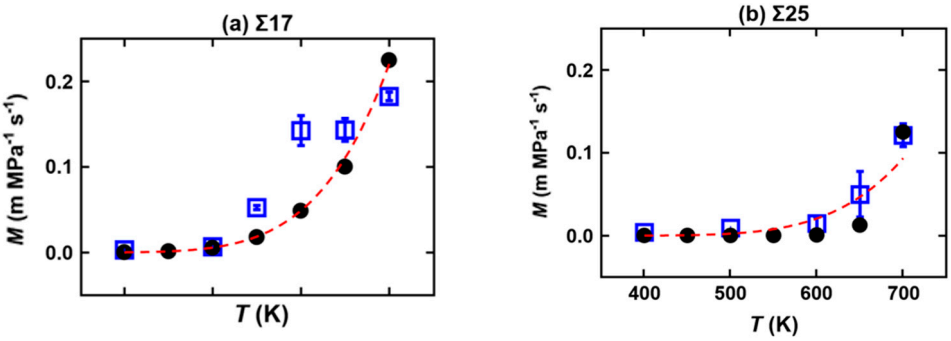

Figure 4. The temperature dependence of GB mobility obtained from the MD simulations (blue squares), kMC simulations (black circles) and fracture models (red lines) for Al (**a**) Σ17 [100] (035) and (**b**) Σ25 [100] (034) symmetric rhombohedral grain boundaries, where the hollow blue squares represent their average values. The *x*-axis represents the temperature, and the *y*-axis represents the GB mobility M.

The validation process reflects that molecular dynamics has better accuracy in the description of the mobility of quasi-2D grain boundaries and has continuity in the description of the mobility compared with the kMC and statistical disconnection model, and the parameterization of the statistical disconnection model by MDs has similar prediction results. So, the numerical calculations by the fracture statistical model can greatly reduce the cost of large-scale MD simulations within the allowable range of error. The computational cost of large-scale MD simulations can be greatly reduced.

The interaction between dislocations and GBs plays an important role in the strengthening of metallic systems, crack growth of single-phase or multi-phase ductile metals, fatigue crack growth and stress corrosion cracking [33]. The mechanism of GB strengthening is one of the ways to improve the plastic strength of materials by creating hindrance for dislocations through the interaction between dislocations and GBs. Different modes of interaction have various effects, so there is a need to construct a generalized criterion for predicting the type of interaction and evaluating the hindering effect [34].

In A. Kedharnath's MD study of the motion of tantalum dislocations on grain boundaries [34], 32 slip configurations totaling 64 structures were constructed on two crystal planes by twisting neighboring grains at different angles around the grain plane axis. Firstly, numerical calculations of the resolved shear stress (RSS) at GBs were made using the slip transfer parameters (STPs) and then MDs were carried out for the 64 configurations. The potential function used is the interatomic potential of the tungsten–tantalum system developed by Chen et al. by fitting the data from experiments and first principles calculations [35]; finally, the results obtained by MDs and STPs were used as the input parameters, and the RSS at the GBs were used as the output parameters. The relationships between the data were fitted by the machine learning model XGBoost [36], and the model parameters were explained by SHAP [37] to interpret the model parameters. This step aims to obtain the degree of influence of the descriptors on the model in order to obtain the correlation between the input and the output. By machine learning combined with numerical calculations and MD simulation parameters, we can predict more macroscopic properties of GBs.

It was found that some of the parameters can quantify the RSS more accurately, including the parameter absorption of a dislocation Dcr, drop in shear stress $\Delta\tau$ in MDs and m' in the calculation of STPs,

$$m' = (n_{\text{in}} \cdot n_{\text{out}})(b_{\text{in}} \cdot b_{\text{out}}) = \cos\psi\cos\kappa \tag{4}$$

where n_{in}, b_{in} are fixed grain vectors and n_{out}, b_{out} are torsion grain vectors. The prediction results found that the configurations with a Dcr less than 40 Å and higher $\Delta\tau$ values are difficult to deform compared to the other configurations, with the highest grain boundary yield stress on the [111] face, followed by [112] and [110].

Currently, kinetic calculations in GBs are not limited to MDs, but numerical calculations and the kMC can be complementary to MDs in the study of kinetic properties. Machine learning is a fitting tool in this process to compare the accuracy of different methods. This facilitates the screening of different descriptors to establish a connection between the properties of matter at different scales. However, the accuracy of the methods themselves is still controversial, especially the potential function of MDs, which is not calculated with high accuracy in some models with low symmetry.

2.3. Machine Learning for Computational Efficiency

The cross-scale study of materials has always been a concern, especially characterizing the atomic-scale structure accurately. DFT based on first principles can obtain reliable results in the system of up to a few hundred atoms, and can be used for exploring and screening unknown material structures, but are limited by the computational cost, which makes it difficult to realize kinetic calculations at larger scales; MDs based on the potential model of inter-atomic interactions extends the computational scales but is not as reliable as DFT calculations in terms of accuracy [38]. There are two current applications of machine learning to DFT and MDs: One is to use it as a tool for fitting data, utilizing the good interpolation ability to predict the structure and thermodynamic properties of substances. The other is to extract reference data from DFT, and the potential energy surface (PES) formed by fitting potentials by machine learning can be used to perform calculations close to the accuracy of DFT on larger scales while being comparable to general empirical potentials in terms of the computational cost.

Tamura et al. used both the DFT results of GBs and atoms as a training dataset when exploring the structure of GBs and their properties [39]. They divided the total energy of the DFT system into the localized energy of the GBs so that the results of the DFT can be fully utilized to effectively extract the charge redistribution features at the defects and refine the analysis of the energy distribution at GBs. The latest machine learning model can describe the local energy of grain boundaries accurately and quickly.

As shown in Figure 5, because the local energies will be affected by the kinetic measure, in this paper, they calculate the Bader region energy of the charge density as single-atom energy by using the DFT-PAW method [40] when dividing the local energies. The algorithm adopts LASSO regression, which is a linear model that reduces the model complexity by introducing the regularization parameter λ. It has a better predictive ability and interpretability compared with linear regression models, and it has a better predictive effect for the sparse sample set where the feature size is larger than the sample size. In the optimization algorithm, two penalty terms are introduced:

$$\overset{\sim}{\lambda}^{\text{com}} \parallel \widetilde{\boldsymbol{w}} \parallel_1 + \lambda^{\text{atom}} \parallel \boldsymbol{v} \parallel_1 + \gamma \sum_{k=1}^{N} \left(E_k^{\text{GB}} - \frac{\sum_{i=1}^{M_k} \left(\overset{\sim}{\boldsymbol{w}}^{\top} \boldsymbol{x}_i + \tilde{w}^{0} - E^{\text{bulk}} \right)}{2S_k} \right)^2 \tag{5}$$

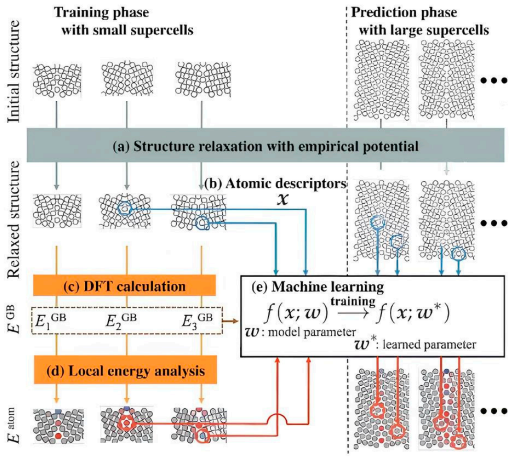

Figure 5. A flowchart of the study by Tamura et al. (**a**) Structures are optimized by empirical potential (**b**) obtain atomic descriptors (**c**) a single-point energy calculation is performed for the grain boundaries, after which (**d**) the calculated energy is divided into the local energies of the atoms. (**e**) model parameters are optimized via machine learning, * represents that this bias parameter is the result of machine learning training.

$\lambda^{\sim com}$, λ^{atom} are two trade-off parameters to improve the prediction accuracy of atomic energies, and γ is a hyperparametric term controlling the strength of the penalty factor to improve the prediction accuracy of grain boundary energies. As shown in Figure 6, where LASSO-aGc uses an optimization algorithm that introduces two penalty terms, the performance is superior to the original LASSO-a algorithm and the LASSO-aG algorithm that only adds an atomic energy correction term. Moreover, the energy bias of all predictions is decreased with the use of the smoothed overlap of atomic positions (SOAP) [41] descriptor.

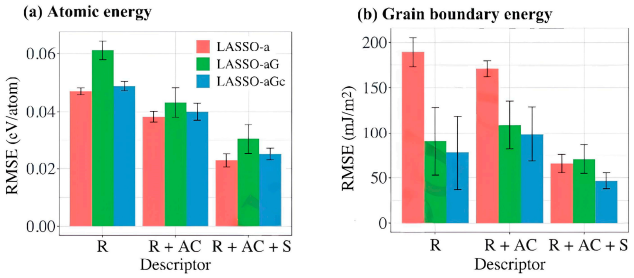

Figure 6. The RMSE of LASSO for the (**a**) single-atom energy and (**b**) grain boundary energy using different descriptors and optimization algorithms. The color represents a different model, and the *x*-axis represents a different descriptor. R is three body angles; AC is the common neighbor analysis (CNA); and S is the smoothed overlap of atomic positions (SOAP).

In this article, the use of multiple configurations (single atoms and GBs) on the sampling achieves an accuracy close to that of DFT with a lower computational cost and enables better results at local energies. The multi-configuration sample space sampling is also used in the training of generalized MLP. In addition, the impact of descriptors on the predictive ability of the model is emphasized in this article, which inspires us to take into account the impact of descriptors for different configurations and also poses a challenge for constructing a generalized MLP.

In Christoph Dösinger et al.'s study, they used active learning for GB deviation in rhenium–tungsten alloys [42]. There are three machine learning methods, and four descriptors were used to learn a DFT dataset, and the Gaussian process regression (GPR) model was found to have the best predictive properties, which employs the Steinhardt parameter as the local environment of the deviated point location. Then, they used Minimization of

the determinant of the Fisher information matrix and of the model prediction error as a criterion, to improve the quality of the model, as it can only use a small amount of new data.

All the research methods provided in the above literature have accomplished the prediction and high-throughput calculation of the energy at GBs with DFT accuracy; meanwhile, they used a small sample space. These methods facilitate the understanding of the energy and structural properties of GBs as well as the exploration of new configurations. The methods were performed only on small-scale systems, and not much more exploration was performed on longer time and larger system scales, which means no bridge from thermodynamics to dynamics has been built in the study. But the machine learning strategy used in the paper and their choice of descriptors provide ideas for constructing MLP with better generalization.

Poul et al. carried out an MLP study of magnesium metal defects [43]. The model they used was the moment tensor potential (MTP) [44], where the "level" affects the number of fitted parameters. Because the energy of atoms in GBs and defects differs from that of a general structure significantly, when constructing a multi-space group dataset without specific defect configurations using $R_{AND}S_{PG}$ [45], DFT relaxation calculations were performed for the initial configurations under low convergence parameters for the volume, cell shape and internal coordinates, respectively, which were used to preserve some of the space group configurations and improve the dataset dimensionality. As shown in Figure 7, the predicted values for GB defects are more accurate as the number of fitted parameters increases. Moreover, in the active learning validation, 100 ps of molecular dynamics calculations were performed for the four conformations to select new conformations for learning.

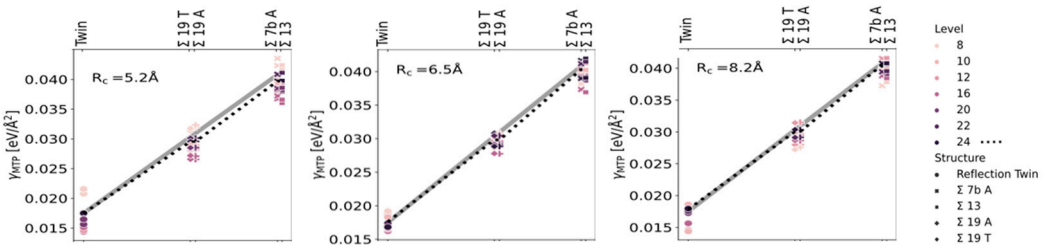

Figure 7. The plot of the defect excess energy prediction for each face at a different cutoff radius (R_c), where the different points represent the prediction of the MTP model using different levels. The dotted line connects the points of potentials with level 24.

In conclusion, the work of Fujii et al. [46]. verifies that the machine learning potential has a large breakthrough in simulation accuracy, and they provide important ideas for efficient material property measurements by comparing the data analysis methods of perturbed MDs and phonon wave-packet simulations.

The thermal conductivity of the silicon lattice in electronic components affects the thermal performance of the electronic component, and the thermal conductivity of single crystal silicon is high. Due to the presence of a large number of grain boundaries in widely used nanoscale silicon [47], which leads to a reduction in thermal conductivity, component heat dissipation problems are triggered. Fujii et al. [46] utilized the MLP library from Kyoto University and obtained the optimal MLP in the library by a grid search in order to calculate the thermal conductivity of silicon GBs. As can be seen in Table 1, the Pareto-optimal machine learning potential (MLP-1) and its potential function developed based on the GB structure data (MLP-2) are able to better represent the GB structure and achieve an accuracy closer to the first principles than the empirical potentials of Tensoff and Stillinger Weber and values similar to the DFT in calculating lattice thermal conductivity. The final four configurations were not included in the dataset. For the configurations that were not known, the errors of all four models increased to varying degrees. However, the error growth of MLP-2 was less than that of the other models, indicating that MLP-2 has superior generalization capabilities.

Table 1. GB energies after relaxation using different potential functions.

GB Type	GB Energy Predict by Different Potential (mJ/m^2)				Reference (mJ/m^2)
-	SW	Tensoff	MLP-1	MLP-2	DFT
$\Sigma3(112)/[1\bar{1}0]$	931	803	757	715	674
$\Sigma3(112)/[1\bar{1}0]$	702	698	758	433	375
$\Sigma5(310)/[001]$	661	629	622	387	333
$\Sigma21(1\bar{5}4)/[111]$	811	795	699	575	534
$\Sigma11(113)/[1\bar{1}0]$	874	881	916	722	676
$\Sigma5(210)/[001]$	673	649	604	409	361
$\Sigma9(112)/[1\bar{1}0]$	446	440	462	252	185
$\Sigma19(331)/[110]$	498	496	493	337	285
RMS error	276	253	250	52	—

The perturbed MD method was used for the GB thermal conductivity test, and the results are shown in Figure 8. Both potential functions reflect the influence of the structure on the thermal conductivity, and the effect is similar, but MLP-2 is closer to the single-crystal thermal conductivity in the test. Moreover, the phonon wave-packet simulations revealed that anharmonic vibrations are also one of the important factors affecting the thermal conductivity of silicon GBs.

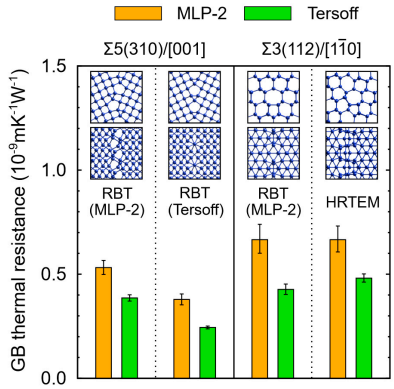

Figure 8. Predicted values of thermal conductivity for different grain boundary models using MLP-2 and Tersoff.

Dai et al. investigated the segregation behavior of tungsten at the GBs of zirconium diboride and the effect of this segregation on the strength of GBs by deep learning potential (DLP) [48–50]. The dataset contains AIMD data for crystals, surfaces and GBs, as shown in Figure 9, and the accuracy of the DFT is realized.

The fitted DLP was applied to the Monte Carlo and MDs to explore the distribution of W in ZrB2 GBs and its effect on material properties: The W-polarization of tungsten in ZrB2 GBs to the equilibrium state is first simulated by the Monte Carlo method, where DLP is used for the determination of the system energy after the atomic exchange; after that, the mechanical strength of GBs is determined by the MD tensile test, and DLP is used for the calculation of the interatomic forces. The results show that the polarization of tungsten enhances the structural stability of grain boundaries at high temperatures, and the polarization of W significantly improves the strength of grain boundaries at temperatures up to 2000 K, which is of great significance for the design and optimization of ultrahigh-temperature ceramics.

The above results show that DLP can better describe the high-temperature system, which proves the potential application of this method in the design of high-temperature materials. It should be noted that due to the drastic changes in the high-temperature system, the temperature gradient and time step should be reduced to improve the quality of the dataset during the AIMD sampling process. Meanwhile, compared with MTP,

DLP also suffers from poor interpretability, i.e., the parameters of DLP have no specific physical meaning.

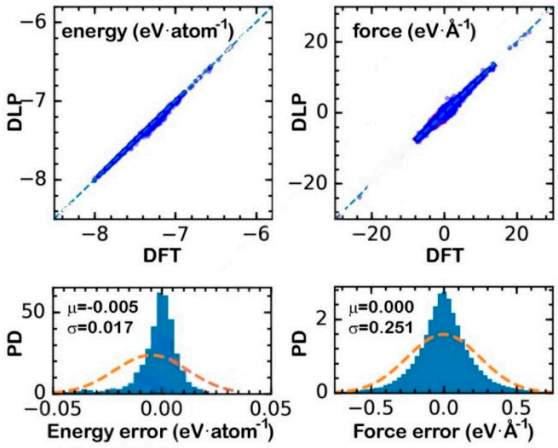

Figure 9. The upper panel shows the energy and force predicted by the DLP on the test set compared to the DFT calculation, and the lower panel shows the probability density (PD) distribution of the prediction error, where the blue part is PD and the yellow line is the fitted normal distribution curve.

3. Challenges and Perspective

There are two challenges for DFT: Firstly, first principles calculations are inherently difficult to use to simulate the dynamic processes of particles. As the dynamic process simulation is to calculate the initial and final states through the energy relaxation to determine the most stable structure, its calculation of the intermediate state reference value is not high. Therefore, how to calculate the transition state and the transformation of a point calculation into a line calculation is necessary for further research. Secondly, existing models are not at the scale of real materials. The number of atoms in the models ranges from tens to hundreds and remains at the microscopic scale. This produces a disconnect between the microscopic lattice and the macroscopic predictions of the material. Combining microstructures with macroscopic properties and establishing universal connections between multiple scales requires continued efforts by researchers.

When training the MLP, the cutoff radius in the descriptor includes only the first few coordination layers, which is a very successful method for materials dominated by covalent and metallic bonds, but the accuracy of this method decreases when long-range interactions dominate, mainly in the ionic solid system. Deep Potential Long-Range (DPLR), developed by Linfeng Zhang et al., corrects for long-range electrostatic interactions between valence electrons [51]. It is approximated by spherical Gaussian charges located on the ions and valence electrons and calculated by Ewald summation, where the position of the valence electrons is fixed at the Wannier center of maximum localization. The Wannier centroid of all valence electrons of each atom depends only on the configuration of its immediate neighbors [52]. However, a framework that would "learn" all long-range terms and hierarchically combine this with a short-range fit, thereby making it generally applicable to all kinds of solids (in particular, weakly ionic ones), is lacking so far [38].

The current trained MLPs have poor extrapolation, i.e., poor prediction of unknown configurations, and may cause overfitting if too many of the same type of data exist in the dataset, which is an inherent characteristic of high-dimensional fitting functions. Therefore, we need to carefully configure the sample space and choose reasonable descriptors. In the generalized α-phase iron-hydrogen embrittlement MTP constructed by Fan-Shun Meng et al. [53], they sampled pure iron, pure hydrogen and their binary system, which included a variety of configurations, such as grain boundaries and clusters. Transfer learning can also be applied to the multivariate system. These methods provide us with ideas to improve the model accuracy and generalization ability.

4. Conclusions

Computer calculation has been widely used in GB research, particularly for materials that are difficult to access or are highly hazardous. Compared to general experimental methods, simulations can obtain thermodynamic information under extreme conditions, and the field of materials science has obtained more detailed structural information about grain boundary structures through simulation calculations over the past decade or so [54]. However, simulations are not particularly generalizable, and in DFT, different exchange correlation functions must be selected according to the specific research system in question; in machine learning, multiple models are often required for comparative analyses, which raises questions about their credibility. Although simulations can facilitate research progress, they still require relevant experiments for validation.

Author Contributions: Conceptualization, L.P. and C.P.; methodology, Y.L.; validation, M.Z., Y.L. and L.L.; formal analysis, L.P. and C.P.; investigation, L.P. and C.P.; writing—original draft preparation, L.P. and C.P.; writing—review and editing, L.P. and C.P.; visualization, L.P. and C.P.; supervision, M.Z., Y.L. and L.L. All authors have read and agreed to the published version of the manuscript.

Funding: This research received no external funding.

Institutional Review Board Statement: Not applicable.

Informed Consent Statement: Not applicable.

Data Availability Statement: Data are contained within the article.

Conflicts of Interest: The authors declare no conflicts of interest.

References

1. Ghamarian, I.; Samimi, P.; Rohrer, G.S.; Collins, P.C. Determination of the Five Parameter Grain Boundary Character Distribution of Nanocrystalline Alpha-Zirconium Thin Films Using Transmission Electron Microscopy. *Acta Mater.* **2017**, *130*, 164–176. [CrossRef]
2. Liu, X.; Chen, Y.; Lu, Y.; Han, J.; Xu, W.; Guo, Y.; Yu, J.; Wei, Z.; Wang, C. Present Research Situation and Prospect of Multi-Scale Design in Novel Co-Based Superalloys: A Review. *Acta Metall. Sin.* **2020**, *56*, 1–20. [CrossRef]
3. Xu, W.W.; Han, J.J.; Wang, Z.W.; Wang, C.P.; Wen, Y.H.; Liua, X.J.; Zhu, Z.Z. Thermodynamic, Structural and Elastic Properties of Co3X (X = Ti, Ta, W, V, Al) Compounds from First-Principles Calculations. *Intermetallics* **2013**, *32*, 303–311. [CrossRef]
4. Shang, S.-L.; Zhou, B.-C.; Wang, W.Y.; Ross, A.J.; Liu, X.L.; Hu, Y.-J.; Fang, H.-Z.; Wang, Y.; Liu, Z.-K. A Comprehensive First-Principles Study of Pure Elements: Vacancy Formation and Migration Energies and Self-Diffusion Coefficients. *Acta Mater.* **2016**, *109*, 128–141. [CrossRef]
5. Zheng, G.; Wang, Q.; Chen, J.; Qiu, R.; Zhu, M. Quantifying Local Atomic Distortions in UO_2 Grain Boundaries: Correlation with Energetic and Electronic Properties. *Inorg. Chem.* **2023**, *62*, 16047–16058. [CrossRef] [PubMed]
6. Li, L.; Zhu, M.; Zheng, G.; Li, Y.; Yang, Y.; Liu, Y.; Su, H. First-Principles Study on the Adsorption Behavior of O_2 on the Surface of Plutonium Gallium System. *Materials* **2022**, *15*, 5035. [CrossRef] [PubMed]
7. Liu, Z.; Wang, Y.; Vaidya, S.; Ruehle, F.; Halverson, J.; Soljačić, M.; Hou, T.Y.; Tegmark, M. KAN: Kolmogorov-Arnold Networks. *arXiv* **2024**, arXiv:2404.19756.
8. Poncé, S.; Li, W.; Reichardt, S.; Giustino, F. First-Principles Calculations of Charge Carrier Mobility and Conductivity in Bulk Semiconductors and Two-Dimensional Materials. *Rep. Prog. Phys.* **2020**, *83*, 036501. [CrossRef]
9. Hermann, J.; DiStasio, R.A., Jr.; Tkatchenko, A. First-Principles Models for van Der Waals Interactions in Molecules and Materials: Concepts, Theory, and Applications. *Chem. Rev.* **2017**, *117*, 4714–4758. [CrossRef]
10. Weng, H.; Dai, X.; Fang, Z. Topological Semimetals Predicted from First-Principles Calculations. *J. Phys.-Condes. Matter* **2016**, *28*, 303001. [CrossRef]
11. Urban, A.; Seo, D.-H.; Ceder, G. Computational Understanding of Li-Ion Batteries. *npj Comput. Mater.* **2016**, *2*, 16002. [CrossRef]
12. Hu, C.; Xia, K.; Fu, C.; Zhao, X.; Zhu, T. Carrier Grain Boundary Scattering in Thermoelectric Materials. *Energy Environ. Sci.* **2022**, *15*, 1406–1422. [CrossRef]
13. Raabe, D.; Herbig, M.; Sandloebes, S.; Li, Y.; Tytko, D.; Kuzmina, M.; Ponge, D.; Choi, P.-P. Grain Boundary Segregation Engineering in Metallic Alloys: A Pathway to the Design of Interfaces. *Curr. Opin. Solid State Mat. Sci.* **2014**, *18*, 253–261. [CrossRef]
14. Feng, B.; Hojo, H.; Mizoguchi, T.; Ohta, H.; Findlay, S.D.; Sato, Y.; Shibata, N.; Yamamoto, T.; Ikuhara, Y. Atomic Structure of a Σ3 [110]/(111) Grain Boundary in CeO_2. *Appl. Phys. Lett.* **2012**, *100*, 073109. [CrossRef]
15. Shibata, N.; Oba, F.; Yamamoto, T.; Ikuhara, Y. Structure, Energy and Solute Segregation Behaviour of [110] Symmetric Tilt Grain Boundaries in Yttria-Stabilized Cubic Zirconia. *Philos. Mag.* **2004**, *84*, 2381–2415. [CrossRef]

16. Suzuki, A.; Mishin, Y. Atomistic Modeling of Point Defects and Diffusion in Copper Grain Boundaries. *Interface Sci.* **2003**, *11*, 131–148. [CrossRef]
17. Mao, Z.G.; Sinnott, S.B.; Dickey, E.C. Ab Initio Calculations of Pristine and Doped Zirconia Σ5 (310)/[001] Tilt Grain Boundaries. *J. Am. Ceram. Soc.* **2002**, *85*, 1594–1600. [CrossRef]
18. Marinopoulos, A.G. First Principles Study of Segregation to the Σ5(310) Grain Boundary of Cubic Zirconia. *J. Phys.-Condes. Matter* **2011**, *23*, 085005. [CrossRef]
19. Feng, B.; Sugiyama, I.; Hojo, H.; Ohta, H.; Shibata, N.; Ikuhara, Y. Atomic Structures and Oxygen Dynamics of CeO_2 Grain Boundaries. *Sci. Rep.* **2016**, *6*, 20288. [CrossRef]
20. Williams, N.R.; Molinari, M.; Parker, S.C.; Storr, M.T. Atomistic Investigation of the Structure and Transport Properties of Tilt Grain Boundaries of UO_2. *J. Nucl. Mater.* **2015**, *458*, 45–55. [CrossRef]
21. Grimmer, H. Coincidence-Site Lattices. *Acta Crystallogr. Sect. A* **1976**, *32*, 783–785. [CrossRef]
22. Bourasseau, E.; Onofri, C.; Ksibi, A.; Iltis, X.; Belin, R.C.; Lapertot, G. Atomic Structure of Grain Boundaries in UO_2 Bicrystals: A Coupled High Resolution Transmission Electron Microscopy/Atomistic Simulation Approach. *Scr. Mater.* **2022**, *206*, 114191. [CrossRef]
23. Wei, J.; Ogawa, T.; Feng, B.; Yokoi, T.; Ishikawa, R.; Kuwabara, A.; Matsunaga, K.; Shibata, N.; Ikuhara, Y. Direct Measurement of Electronic Band Structures at Oxide Grain Boundaries. *Nano Lett.* **2020**, *20*, 2530–2536. [CrossRef]
24. Ashby, M.F.; Spaepen, F.; Williams, S. The Structure of Grain Boundaries Described as a Packing of Polyhedra. *Acta Metall.* **1978**, *26*, 1647–1663. [CrossRef]
25. Dickey, E.C.; Fan, X.; Yong, M.; Sinnott, S.B.; Pennycook, S.J. Atomic Scale Analysis of Cubic Zirconia Grain Boundaries. In *Advances in Materials Problem Solving with the Electron Microscope, Proceedings of the MRS Symposuim Proceeding, Boston, MA, USA, 30 November–3 December 1999*; Bentley, J., Allen, C., Dahmen, U., Petrov, I., Eds.; Materials Research Society: Warrendale, PA, USA, 2001; Volume 589, pp. 323–328.
26. Hojo, H.; Mizoguchi, T.; Ohta, H.; Findlay, S.D.; Shibata, N.; Yamamoto, T.; Ikuhara, Y. Atomic Structure of a CeO_2 Grain Boundary: The Role of Oxygen Vacancies. *Nano Lett.* **2010**, *10*, 4668–4672. [CrossRef]
27. Yan, J.; Shi, R.; Wei, J.; Li, Y.; Qi, R.; Wu, M.; Li, X.; Feng, B.; Gao, P.; Shibata, N.; et al. Nanoscale Localized Phonons at Al2O3 Grain Boundaries. *Nano Lett.* **2024**, *24*, 3323–3330. [CrossRef] [PubMed]
28. Yu, H.L.; Tang, T.; Zheng, S.T.; Shi, Y.; Qiu, R.Z.; Luo, W.H.; Meng, D.Q. A Theoretical Study of Hydrogen Atoms Adsorption and Diffusion on PuO_2 (110) Surface. *J. Alloys Compd.* **2016**, *666*, 287–291. [CrossRef]
29. Turnbull, D. Theory of Grain Boundary Migration Rates. *Trans. Am. Inst. Min. Metall. Eng.* **1951**, *191*, 661–665. [CrossRef]
30. Watanabe, T.; Tsurekawa, S. The Control of Brittleness and Development of Desirable Mechanical Properties in Polycrystalline Systems by Grain Boundary Engineering. *Acta Mater.* **1999**, *47*, 4171–4185. [CrossRef]
31. Chen, K.; Han, J.; Srolovitz, D.J. On the Temperature Dependence of Grain Boundary Mobility. *Acta Mater.* **2020**, *194*, 412–421. [CrossRef]
32. Homer, E.R.; Holm, E.A.; Foiles, S.M.; Olmsted, D.L. Trends in Grain Boundary Mobility: Survey of Motion Mechanisms. *Jom* **2014**, *66*, 114–120. [CrossRef]
33. Kacher, J.; Eftink, B.P.; Cui, B.; Robertson, I.M. Dislocation Interactions with Grain Boundaries. *Curr. Opin. Solid State Mater. Sci.* **2014**, *18*, 227–243. [CrossRef]
34. Gravell, J.D.; Cho, J.; Lee, S.; Aubry, S.; Ryu, I. Prediction of Dislocation—Grain Boundary Interactions in FCC Aluminum Bicrystals Using a Modified Continuum Criterion and Machine Learning Methods. *Materialia* **2023**, *31*, 101874. [CrossRef]
35. Chen, Y.; Fang, J.; Liu, L.; Hu, W.; Gao, N.; Gao, F.; Deng, H. Development of the Interatomic Potentials for W-Ta System. *Comput. Mater. Sci.* **2019**, *163*, 91–99. [CrossRef]
36. Chen, T.; Guestrin, C. XGBoost: A Scalable Tree Boosting System. In Proceedings of the 22nd ACM SIGKDD International Conference on Knowledge Discovery and Data Mining, Association for Computing Machinery, San Francisco, CA, USA, 13–17 August 2016; pp. 785–794.
37. Lundberg, S.M.; Lee, S.-I. A Unified Approach to Interpreting Model Predictions. In Proceedings of the 31st International Conference on Neural Information Processing Systems, Long Beach, CA, USA, 4–9 December 2017; pp. 4768–4777.
38. Deringer, V.L.; Caro, M.A.; Csányi, G. Machine Learning Interatomic Potentials as Emerging Tools for Materials Science. *Adv. Mater.* **2019**, *31*, 1902765. [CrossRef] [PubMed]
39. Tamura, T.; Karasuyama, M.; Kobayashi, R.; Arakawa, R.; Shiihara, Y.; Takeuchi, I. Fast and Scalable Prediction of Local Energy at Grain Boundaries: Machine-Learning Based Modeling of First-Principles Calculations. *Model. Simul. Mater. Sci. Eng.* **2017**, *25*, 075003. [CrossRef]
40. Seko, A. Sparse Representation for a Potential Energy Surface. *Phys. Rev. B* **2014**, *90*, 024101. [CrossRef]
41. Caro, M.A. Optimizing Many-Body Atomic Descriptors for Enhanced Computational Performance of Machine Learning Based Interatomic Potentials. *Phys. Rev. B* **2019**, *100*, 024112. [CrossRef]
42. Doesinger, C.; Hodapp, M.; Peil, O.; Reichmann, A.; Razumovskiy, V.; Scheiber, D.; Romaner, L. Efficient Descriptors and Active Learning for Grain Boundary Segregation. *Phys. Rev. Mater.* **2023**, *7*, 113606. [CrossRef]
43. Poul, M.; Huber, L.; Bitzek, E.; Neugebauer, J. Systematic Atomic Structure Datasets for Machine Learning Potentials: Application to Defects in Magnesium. *Phys. Rev. B* **2023**, *107*, 104103. [CrossRef]

44. Avery, P.; Zurek, E. RandSpg: An Open-Source Program for Generating Atomistic Crystal Structures with Specific Spacegroups. *Comput. Phys. Commun.* **2017**, *213*, 208–216. [CrossRef]
45. Shapeev, A.V. Moment Tensor Potentials: A Class of Systematically Improvable Interatomic Potentials. *Multiscale Model. Simul.* **2016**, *14*. [CrossRef]
46. Fujii, S.; Seko, A. Structure and Lattice Thermal Conductivity of Grain Boundaries in Silicon by Using Machine Learning Potential and Molecular Dynamics. *Comput. Mater. Sci.* **2022**, *204*, 111137. [CrossRef]
47. Nakamura, Y.; Isogawa, M.; Ueda, T.; Yamasaka, S.; Matsui, H.; Kikkawa, J.; Ikeuchi, S.; Oyake, T.; Hori, T.; Shiomi, J.; et al. Anomalous Reduction of Thermal Conductivity in Coherent Nanocrystal Architecture for Silicon Thermoelectric Material. *Nano Energy* **2015**, *12*, 845–851. [CrossRef]
48. Zhang, L.; Han, J.; Wang, H.; Car, R.; Weinan, E. Deep Potential Molecular Dynamics: A Scalable Model with the Accuracy of Quantum Mechanics. *Phys. Rev. Lett.* **2018**, *120*, 143001. [CrossRef]
49. Wang, H.; Zhang, L.; Han, J.; E., W. DeePMD-Kit: A Deep Learning Package for Many-Body Potential Energy Representation and Molecular Dynamics. *Comput. Phys. Commun.* **2018**, *228*, 178–184. [CrossRef]
50. Dai, F.-Z.; Wen, B.; Xiang, H.; Zhou, Y. Grain Boundary Strengthening in ZrB2 by Segregation of W: Atomistic Simulations with Deep Learning Potential. *J. Eur. Ceram. Soc.* **2020**, *40*, 5029–5036. [CrossRef]
51. Zhang, L.; Wang, H.; Muniz, M.C.; Panagiotopoulos, A.Z.; Car, R.; E., W. A Deep Potential Model with Long-Range Electrostatic Interactions. *J. Chem. Phys.* **2022**, *156*, 124107. [CrossRef]
52. Zhang, L.; Chen, M.; Wu, X.; Wang, H.; Weinan, E.; Car, R. Deep Neural Network for the Dielectric Response of Insulators. *Phys. Rev. B* **2020**, *102*, 041121. [CrossRef]
53. Meng, F.-S.; Du, J.-P.; Shinzato, S.; Mori, H.; Yu, P.; Matsubara, K.; Ishikawa, N.; Ogata, S. General-Purpose Neural Network Interatomic Potential for the α-Iron and Hydrogen Binary System: Toward Atomic-Scale Understanding of Hydrogen Embrittlement. *Phys. Rev. Mater.* **2021**, *5*, 113606. [CrossRef]
54. Hong, C.; Choi, J.M.; Jeong, W.; Kang, S.; Ju, S.; Lee, K.; Jung, J.; Youn, Y.; Han, S. Training Machine-Learning Potentials for Crystal Structure Prediction Using Disordered Structures. *Phys. Rev. B* **2020**, *102*, 224104. [CrossRef]